Geochemical Perspectives Letters

Contrasting controls on $\delta^{18}O$-$\delta^{2}H$ and $\delta^{18}O$-$\delta^{17}O$ systematics in a balance filled lake

M.J. Custado[1,2*], A.R. Waldeck[1,3], B. Belanger[4], X.-K. Wang[1], J.C.K. Rugenstein[5], K.M. Cobb[1,2], J.L. Oster[4], D.E. Ibarra[1,2]

Abstract

https://doi.org/10.7185/geochemlet.2631

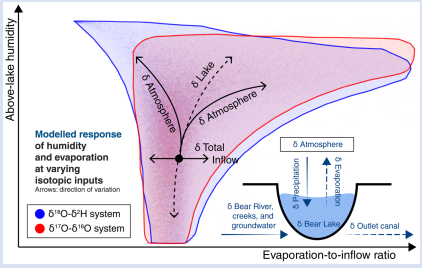

Recent analytical advancements now allow precise quantification of ^{17}O excess ($\Delta'^{17}O$), introducing the triple oxygen isotope system ($\delta^{17}O$-$\delta^{18}O$) as a complementary tool to d-excess, its analogue in the classic $\delta^{18}O$-$\delta^{2}H$ system. Therefore, the objective of this study is to contrast the sensitivities of the $\delta^{18}O$-$\delta^{2}H$ and $\delta^{18}O$-$\delta^{17}O$ systems to varying environmental and isotopic parameters. To do this, we present a new triple oxygen isotope data set from the Bear River watershed (Utah/Idaho, USA) and model lake evaporation trajectories using Monte Carlo driven steady state mass balance modelling. Results demonstrate that $\Delta'^{17}O$ provides more accurate humidity constraints. Modelling the evaporation trajectories of the balance filled Bear Lake, we show that the uncertainty of the calculated lake isotopic composition increases with increasing evaporation-to-inflow ratio (X_e). This observation implies the need to better constrain isotopic inputs, particularly that of atmospheric moisture, in dry environments where X_e is high. Further, this study highlights the need for a larger $\Delta'^{17}O$ data set aggregation across environmental conditions to better characterise variability and reduce uncertainty in calibrating isotope mass balance models.

Received 1 March 2026 | Accepted 3 August 2026 | Published 8 September 2026

Introduction

Stable isotope hydrology in lakes has traditionally relied on $\delta^{18}O$-$\delta^{2}H$ systematics to constrain lake water balance (Gonfiantini, 1986; Gat, 1995; Gibson *et al.*, 2016). Initially, $\delta^{17}O$ was believed to provide no additional information beyond the $\delta^{18}O$-$\delta^{2}H$ framework. However, analytical advancements now allow the precise quantification of mass dependent fractionation between $\delta^{17}O$ and $\delta^{18}O$, from which an analogue to d-excess, ^{17}O excess ($\Delta'^{17}O$), can be calculated. Previous studies have noted the relative insensitivity of $\Delta'^{17}O$ to temperature compared to d-excess (Angert *et al.*, 2004; Uemura *et al.*, 2010). This characteristic increases the potential of the $\delta^{17}O$-$\delta^{18}O$ system to provide unique hydrological information in both modern (Pierchala *et al.*, 2022; Voigt *et al.*, 2025) and palaeoclimate settings, where it has been used to reconstruct humidity and evaporation conditions (Gázquez *et al.*, 2018; Passey and Ji, 2019; Gázquez-Sánchez *et al.*, 2023; Katz *et al.*, 2023). Its utility may be greatest in studies using mineral archives, particularly authigenic carbonates, where paired $\delta^{2}H$ data cannot be extracted from the same mineral. The introduction of high throughput instruments to measure $\delta^{17}O$ has further enhanced measurement efficiency and precision, supplementing existing tools for palaeoclimate research and modern water management (*e.g.*, Berman *et al.*, 2013; Steig *et al.*, 2021).

In this study, we present a new triple oxygen isotope data set from Bear Lake, Utah/Idaho to derive relative humidity and evaporation-to-inflow ratios. By comparing the triple oxygen and $\delta^{18}O$-$\delta^{2}H$ data from replicates of the same samples (*cf.* Custado *et al.*, 2025), we highlight how each system constrains key parameters, demonstrating the added utility of $\Delta'^{17}O$ in lake balance applications. This work is compared to previous $\Delta'^{17}O$ data from Bear Lake (Passey and Ji, 2019) and comparable modelling for other mid-latitude lakes (Surma *et al.*, 2015, 2018; Gázquez *et al.*, 2018; Voigt *et al.*, 2021, 2025).

Steady State Isotopic Mass Balance Equations

The Craig-Gordon evaporation model is often used to describe isotope exchange at the water-atmosphere interface during evaporation of an open water body (Craig and Gordon, 1965). The kinetic component of this isotopic process can be modelled through molecular diffusion, as predicted by kinetic theory (Criss, 1999). Building on these concepts, the following equation represents the steady state isotopic mass balance of a well mixed, throughflow lake (Craig and Gordon, 1965; Gonfiantini, 1986; Criss, 1999; Gibson *et al.*, 2016; Passey and Levin, 2021):

1. Department of Earth, Environmental, and Planetary Sciences, Brown University
2. Institute at Brown University for Environment and Society, Brown University
3. Department of Geosciences, Pennsylvania State University
4. Department of Earth and Environmental Sciences, Vanderbilt University
5. Department of Geosciences, Colorado State University

* Corresponding author (email: manuel_justin_custado@brown.edu)

$$R_L = \frac{\alpha_{eq}\alpha_{diff}(1-h)R_I + \alpha_{eq}hX_eR_A}{\alpha_{eq}\alpha_{diff}(1-h)(1-X_e) + X_e} \quad \text{Eq. 1}$$

where R represents isotopic (^{17}O, ^{18}O, ^{2}H) compositions expressed in ratios relative to a known standard (Vienna Standard Mean Ocean Water, VSMOW). The subscripts L, A, and I denote the steady state isotopic compositions of the lake, atmospheric moisture, and inflow, respectively. The variable h represents relative humidity normalised to the lake surface temperature, X_e the evaporation-to-inflow ratio, α_{eq} the equilibrium fractionation factor, and α_{diff} the kinetic fractionation at zero humidity (diffusion end member). Note that in Criss (1999), $\alpha_{eq}{\cdot}\alpha_{diff}$ is expressed as α^{0}_{evap}. This work follows the conventions for α in Gonfiantini (1986), where $\alpha > 1$.

We applied Equation 1 to both triple oxygen and $\delta^{18}O$-$\delta^{2}H$ isotope systems. Ratios are preferred in triple oxygen isotopic calculations as $\Delta'^{17}O$ is derived from linearised isotopic data (δ'; Eq. 2; Miller, 2002; Luz and Barkan, 2010):

$$\delta' = \ln(R) \quad \text{Eq. 2}$$

A full description of the equations is provided in the Supplementary Information.

Study Site

Bear Lake lies within the semi-arid northeast Great Basin, bounded by the Bear Lake Plateau and Bear River Range (Fig. 1). The lake is primarily fed by the Bear River through an inlet canal, whose headwaters are located further south in the Uinta Mountains. Surrounding creeks and springs provide additional input, particularly those originating from the Bear River Range. Groundwater is estimated to have a minor contribution (Bright, 2009; Custado *et al.*, 2025). Most precipitation falls as snow, which reaches the lake through immediate and delayed snowmelt *via* streams. Water exits the lake through evaporation and an outlet canal (Bright, 2009). Annual volumetric discharge of each inflow component is summarised in Table S-1. Additionally, a brief description of the physical and hydroclimatic setting of the lake is provided in the Supplementary Information.

Analytical and Computational Methods

Lake, stream, and groundwater samples were collected during baseflow in August 2023 (Fig. 1) and analysed along with isotopic standards using a Picarro L2140-i cavity ring down spectrometer at Brown University, USA. Precipitation samples were obtained from sampling stations located in Utah State University and Utah Valley University. Analytical drift and memory corrections were applied before data normalisation to the VSMOW-SLAP scale using internally calibrated reference waters (Gröning, 2011; Hutchings and Konecky, 2023).

The second order isotopic parameters are calculated using the following equations:

$$\Delta'^{17}O = \delta'^{17}O - 0.528 \times \delta'^{18}O \quad \text{Eq. 3}$$

$$\text{d-excess} = \delta^{2}H - 8 \times \delta^{18}O \quad \text{Eq. 4}$$

Relative humidity and X_e from each isotope system were derived using Monte Carlo simulations ($n = 100{,}000$) of Equation 1, with input distributions generated from measured isotope data of samples and corresponding analytical uncertainties (Table S-2, Fig. S-1). A detailed description of the computational approach is provided in the Supplementary Information.

Final values reported in Table 1 are the median of the output distributions (Fig. S-2), with uncertainties expressed as the interquartile range (IQR, 25th-75th percentiles). Means and standard deviations (1σ) are reported in Table S-3.

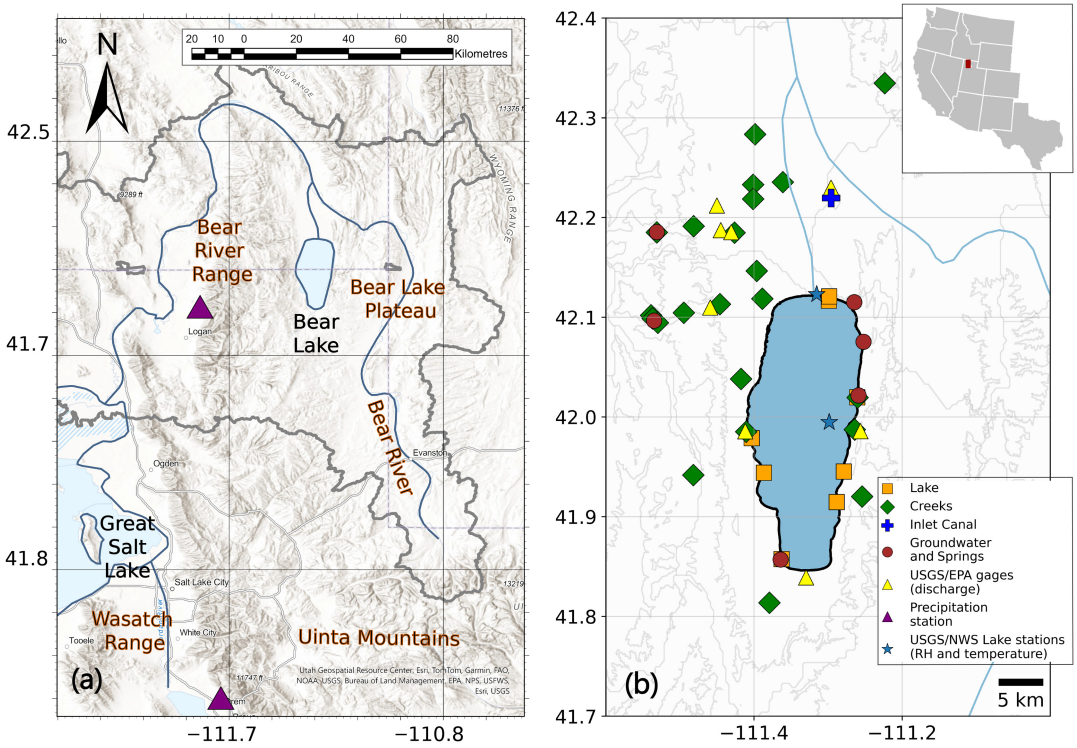

Figure 1 **(a)** Bear River watershed (grey outline) map and **(b)** sampling site locations; inset shows Bear Lake in the western U.S. This study utilised replicate samples from sites shown in panel **(b)** and previously reported by Custado *et al.* (2025).

Table 1 Comparison of calculated relative humidity and X_e. Values are reported as median and IQR from 100,000 Monte Carlo simulations due to the non-normality of the output distributions (Fig. S-2). Mean and 1σ values are in Table S-3.

Isotope system	Calculated *h* from Monte Carlo simulations*	Calculated *h* normalised to air temperature**	Evaporation/ Inflow (X_e)	Sample collection dates	References
Triple oxygen	0.590 *(IQR 0.375–0.774)*	0.532 *(IQR 0.338–0.698)*	0.267 *(IQR 0.231–0.308)*	August 2023	This study
$\delta^{18}O$-$\delta^{2}H$	0.639 *(IQR 0.455–0.788)*	0.577 *(IQR 0.411–0.711)*	0.281 *(IQR 0.240–0.321)*	August 2023	This study
$\delta^{18}O$-$\delta^{2}H$	0.62 ± 0.03	0.56 ± 0.03	0.38 ± 0.01	July 1981 to August 2023	Custado *et al.* (2025)

*Mass balance derived humidity is normalised to lake surface temperature, while instrument derived humidity is normalised to air temperature.
**Temperatures used for conversion: evaporation flux weighted lake (11.16 °C) and air temperature (12.72 °C). See Table S-4 for monthly values.

Isotopic Mass Balance of Bear Lake

Figure 2 illustrates our new isotopic data set in both $\delta'^{18}O$-$\Delta'^{17}O$ and $\delta^{18}O$-d-excess spaces, overlain on evaporation trajectories modelled as a function of X_e at different humidities (Eq. 1).

The volume weighted mean inflow (yellow star, Fig. 2) is composed of inputs from the inlet canal (orange diamond, 55.68 % of total volumetric inflow), on-lake precipitation (purple star, 18.91 %), creeks (orange star, 25.39 %), and groundwater (pink star, 0.01 %). The spread in the $\Delta'^{17}O$ of the inflow components, like d-excess, suggests potential for $\Delta'^{17}O$ to distinguish sources with different evaporation histories, as is the case with this system (inset plots, Fig. 2). For example, Voigt *et al.* (2021) previously demonstrated that $\Delta'^{17}O$ can resolve the evaporation trajectories of shallow lakes with and without recharge in Salar del Huasco, Chile. In contrast, Bear Lake is primarily fed by snowmelt from surrounding mountains, which exhibit a narrower range of d-excess values.

Deriving *h* and X_e from Mass Balance Calculations

Table 1 summarises the mass balance results along with the multi-year data set results of Custado *et al.* (2025).

The calculated uncertainties do not statistically differentiate the values in Table 1, partly due to the conservative approach used to generate input uncertainties, which better captures data variability (see Supplementary Information). Nevertheless, the median triple oxygen derived *h* and X_e are slightly lower than $\delta^{18}O$-$\delta^{2}H$ estimates and comparable to Custado *et al.* (2025). The observed discrepancies likely reflect temporal coverage differences in the data, while analytical uncertainty and data variability account for the modelled uncertainties (Table S-1).

The evaporation flux weighted relative humidity calculated from monthly United States Geological Survey (USGS) observations (Table S-4) is ~0.53, closer to the triple oxygen

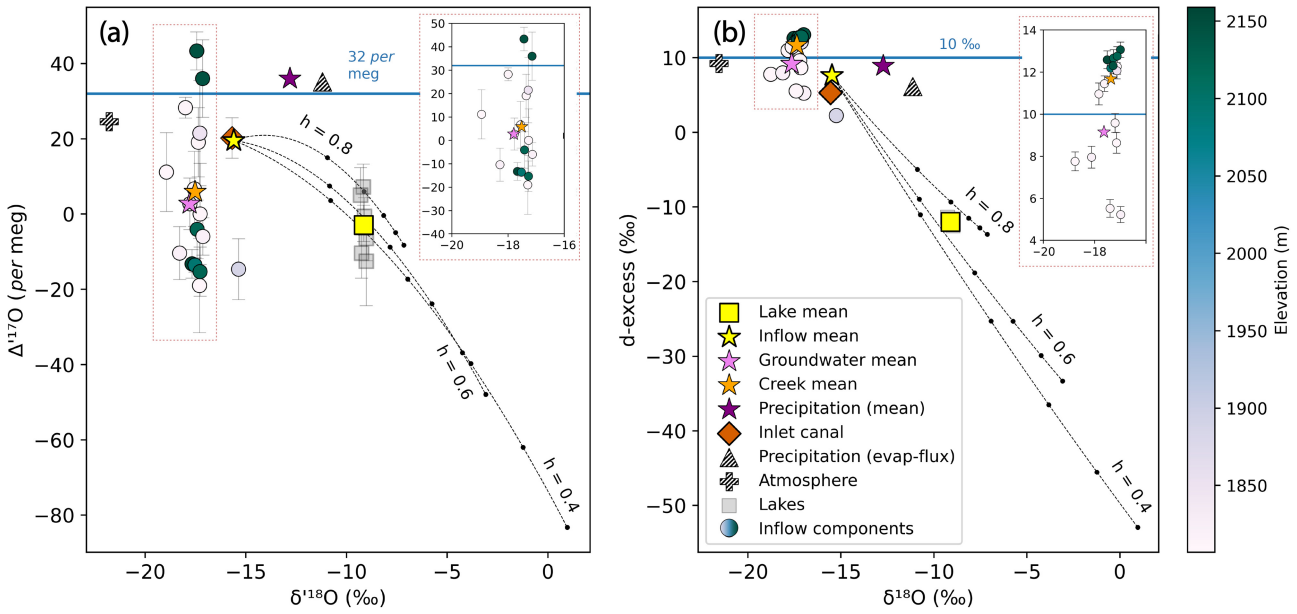

Figure 2 **(a)** $\Delta'^{17}O$ *versus* $\delta'^{18}O$ and **(b)** d-excess *versus* $\delta^{18}O$. Blue lines denote the Global Meteoric Water Line (GMWL), while black dashed lines represent lake isotopic evolution during evaporation at different humidities. Black dots indicate X_e values from 0 to 1 in increments of 0.2. Inflow components (circles) represent individual stream samples and are coloured by elevation; the inlet canal is included in the inflow mean. Insets show magnified views of the areas within the red dashed boxes. Only samples with paired discharge information were used in the calculations. Note that the error bars for d-excess are smaller than the markers. A link to the complete data set is included in the Supplementary Information.

derived median h when normalised to air temperature. This agreement suggests that triple oxygen data may better constrain above lake humidity, even with limited temporal resolution. Oxygen isotopes are generally more sensitive to kinetic fractionation than deuterium (Gonfiantini, 1986) and may therefore better record relative humidity changes. Additionally, the relative insensitivity of $\Delta'^{17}O$ to temperature compared to d-excess allows moisture source effects to be isolated without temperature corrections (Angert *et al.*, 2004; Uemura *et al.*, 2010). However, additional constraints on the input parameters are needed to reduce estimation errors.

Isotopic Controls on h and X_e

Previous studies have highlighted the sensitivity of isotopic mass balance models to varying isotopic and environmental inputs (*e.g.*, Gázquez *et al.*, 2018; Passey and Ji, 2019; Voigt *et al.*, 2021), particularly relative humidity and the isotopic compositions of inflow and atmospheric moisture (Barkan and Luz, 2007; Surma *et al.*, 2015, 2018; Voigt *et al.*, 2021). The influence of salinity and wind turbulence (n), while important, was not explicitly considered; instead a value of n = 0.5, commonly applied to lake studies (Gonfiantini, 1986; Criss, 1999; Gibson *et al.*, 2016), was adopted to correct for the α_{diff} values used (Table S-2). For this work, we focus on parameters that can be constrained given available environmental data. Nevertheless, we provide Figure S-3 to model the response of lake isotopic composition to varying n. Figure 3 summarises how lake isotopic composition, h, and X_e respond to a range of inputs.

In both systems, the spread in the modelled lake isotopic composition increases with X_e (Fig. 3a,b). This pattern is consistent when simulations are focused on separate input parameters, with humidity and isotopic composition of atmospheric moisture having the greatest relative influence at X_e = 1 (Fig. S-4). However, lake isotopic composition responds more strongly to inflow at lower X_e, likely due to less kinetic fractionation at lower evaporation rates (Fig. S-4a,e). Conversely, at higher X_e, the parameters that control the isotopic (δ_A) and moisture (h) gradient above the lake become increasingly important as more vapour escapes from the lake (Craig and Gordon, 1965).

Additionally, both isotope systems feature a triangular solution space for h and X_e (Fig. 3c), with the $\delta^{18}O$-δ^2H system showing greater divergence in X_e at higher h. Consequently, $\Delta'^{17}O$ appears to provide a tighter constraint on relative humidity and its trade off with X_e. Figure S-4 illustrates how this solution space changes when variability is isolated to individual parameters, showing that the spread at high h is primarily governed by δ_A (Fig. S-4). Despite preserving the GMWL relationship between atmospheric $\delta^{18}O$ with δ^2H in the model, the non-unique solutions at high h demonstrates the strong sensitivity of the $\delta^{18}O$-δ^2H system to atmospheric moisture variability.

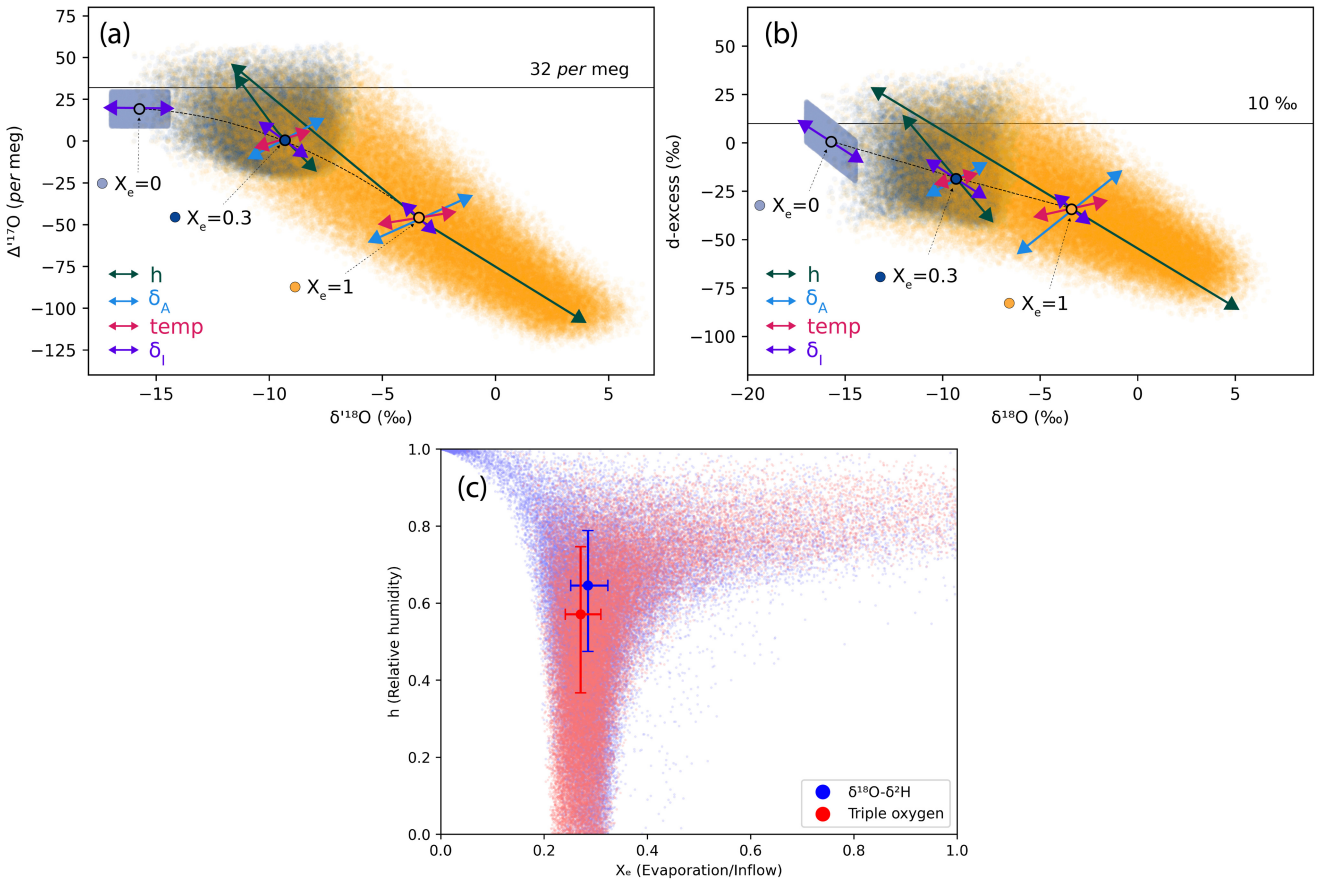

Figure 3 Sensitivity of lake isotopic composition and environmental parameters to varying evaporation conditions. Changes in the lake isotopic composition as a function of X_e are shown in **(a)** $\delta'^{18}O$ *versus* $\Delta'^{17}O$ and **(b)** $\delta^{18}O$ *versus* d-excess spaces, while changes in X_e (x axis) and h (y axis) from varying isotopic inputs are shown in **(c)**. Horizontal lines in **(a)** and **(b)** represent the GMWL. Error bars in **(c)** represent the IQR around the median value (circle). Inputs for **(a)** and **(b)** were h, δ_A, temperature, and δ_I; inputs for **(c)** were δ_A, temperature, δ_I, and lake composition (δ_L). Each marker represents one of 100,000 simulations sampled from normal distributions defined by the calculated input parameter values and uncertainties (see Supplementary Information). Arrows in **(a)** and **(b)** indicate the range of outputs generated by varying a single input while holding others constant (*cf.* Gázquez *et al.*, 2018). Corresponding individual simulations are compiled in Figure S-4.

Previous studies often rely on estimating δ_A due to difficulties in making direct measurements (Surma *et al.*, 2015, 2018; Gázquez *et al.*, 2018; Passey and Ji, 2019; Voigt *et al.*, 2021). Here, we estimated δ_A by assuming that atmospheric moisture upwind of the lake is in equilibrium with evaporation flux weighted mean precipitation, implicitly accounting for seasonality to better reproduce observed lake and inflow isotopic compositions (Eq. S-14; Gibson *et al.*, 2016; Custado *et al.*, 2025). Other studies instead assume complete or partial isotopic equilibrium between atmospheric moisture and inflow waters (Gázquez *et al.*, 2018; Passey and Ji, 2019), with limited existing measurements in continental settings (*e.g.*, Voigt *et al.*, 2021, 2025). Regardless of the chosen approach, fractionation during evaporation has been consistently demonstrated to be sensitive to both δ_A and relative humidity, underscoring the need for more direct measurements of these parameters.

Comparison to Previous Studies

To simulate palaeoclimate applications of $\Delta'^{17}O$ in lakes, we calculated the $\delta'^{17}O$-$\delta'^{18}O$ slope between the source and lake waters (λ_{lake}) using empirical λ_{lake}-$\Delta'^{17}O$ relationships derived by Passey and Ji (2019) and Katz *et al.* (2023), and subsequently, the reconstructed $\delta^{18}O$ of the unevaporated catchment precipitation ($\delta^{18}O_{rucp}$) (Eqs. S-15, S-16). Multiple λ_{lake}-$\delta^{18}O_{rucp}$ pairs were calculated from these empirical equations and compared with values derived directly from measured inflow and lake isotopic data. These values are summarised in Table S-5.

The calculated λ_{lake} values using the empirical coefficients (λ_{lake} = 0.5213 to 0.5235) yielded higher median $\delta^{18}O_{rucp}$ estimates (Table S-5) than the measured stream samples (−18.1 ± 1.4 ‰, Passey and Ji, 2019; −17.2 ± 0.6 ‰ (1σ), this study). In contrast, the λ_{lake} value calculated from measured inflow and lake samples (0.5246) resulted in a $\delta^{18}O_{rucp}$ value of −18.1 ± 5.4 ‰, expectedly lower than the measured stream samples. This discrepancy underscores the importance of additional data from diverse modern lake environments to refine empirical λ_{lake}-$\Delta'^{17}O$ relationships and better constrain inflow water distributions in palaeo-catchments.

Triple oxygen isotope mass balance models have been implemented in semi-permanent freshwater systems in arid environments, where groundwater recharge is of periodic importance (Surma *et al.*, 2015, 2018; Voigt *et al.*, 2021). These studies show that triple oxygen isotopes can distinguish between simple and recharged evaporation. Although Bear Lake currently receives minimal groundwater input, palaeoclimate records indicate that it has alternated between underfilled and overfilled states, implying periods of substantial groundwater influence (Bright, 2009; Dean, 2009; Kaufman *et al.*, 2009). Reconstructions of h and X_e from gypsum hydration waters where the lake balance model simultaneously solves for both isotope systems show that changes in X_e at higher values (>0.75) produce lower variations in the back calculated h (Gázquez *et al.*, 2018). Figure 3c shows that this observation is likely due to the constraints provided by the triple oxygen data. Together with the ability to reconstruct the isotopic composition of the unevaporated source waters, these observations demonstrate the potential of triple oxygen isotopes to provide unique hydrological insights.

Implications

Comparison of triple oxygen and $\delta^{18}O$-$\delta^{2}H$ isotopic systems reveals differing sensitivities to environmental and isotopic inputs when estimating h and X_e. Both systems yielded comparable X_e values, supporting their use in water management applications where quantifying hydrological balance components, such as evaporation, are essential (*e.g.*, Surma *et al.*, 2015; Custado *et al.*, 2025). Simultaneous use of both systems may best constrain multiple parametric unknowns (Gázquez *et al.*, 2018); however, improved monitoring of h and the isotopic composition of atmospheric moisture at the lake surface is necessary to reduce uncertainties in under constrained fluxes, such as evaporation and groundwater discharge, particularly in semi-arid regions where annual X_e values are typically high.

Additionally, patterns in our data suggest that $\Delta'^{17}O$ may be a more consistent recorder of above lake h. This finding supports the growing use of triple oxygen isotopes in palaeoclimate studies, which have been analysed in lacustrine carbonate and gypsum hydration waters to reconstruct past environmental conditions (Gázquez *et al.*, 2018; Passey and Ji, 2019; Katz *et al.*, 2023), and lacustrine chert to reconstruct past elevation (Ibarra *et al.*, 2021). However, mass balance derived h is normalised to lake temperature, making constraints on past lake temperatures important for palaeoclimate reconstructions. As shown in our calculations, even a modest difference between lake air temperatures yields considerably different h estimates (Table 1).

The combined use of $\Delta'^{17}O$ and d-excess has been proposed for tracking moisture sources, leveraging the lower temperature sensitivity of $\Delta'^{17}O$ relative to d-excess (Angert *et al.*, 2004; Uemura *et al.*, 2010). However, its application to reconstruct h and $\delta^{18}O_{rucp}$ requires well constrained isotopic inputs, as demonstrated by the differences between estimates derived from measured samples and empirical relationships. Therefore, this work underscores the need to expand $\Delta'^{17}O$ measurements of meteoric waters across seasons and environmental gradients to better characterise $\delta^{17}O$-$\delta^{18}O$ isotope system fractionation and improve accuracy of mass balance models and empirical relationships, such as those of Passey and Ji (2019) and Katz *et al.* (2023). Additionally, further improvements in analytical precision and throughput (*e.g.*, Hutchings and Konecky, 2023; Terzer-Wassmuth *et al.*, 2023) will also help reduce uncertainty.

Acknowledgements

This work was funded by NSF AGS 2102901 and AGS 2333-173 to DEI, NSF AGS 2333172 to JKCR, NSF AGS 2102884 to JLO, with additional support from the Brown University Division of Research.

Editor: Gavin Foster

Additional Information

Supplementary Information accompanies this letter at https://www.geochemicalperspectivesletters.org/article2631.

Cite this letter as: Custado, M.J., Waldeck, A.R., Belanger, B., Wang, X.-K., Rugenstein, J.C.K., Cobb, K.M., Oster, J.L., Ibarra, D.E. (2026) Contrasting controls on $\delta^{18}O$-$\delta^{2}H$ and

$\delta^{18}O$-$\delta^{17}O$ systematics in a balance filled lake. *Geochem. Persp. Let.* 41, 40–45. https://doi.org/10.7185/geochemlet.2631

References

Angert, A., Cappa, C.D., DePaolo, D.J. (2004) Kinetic ^{17}O effects in the hydrologic cycle: Indirect evidence and implications. *Geochimica et Cosmochimica Acta* 68, 3487–3495. https://doi.org/10.1016/j.gca.2004.02.010

Barkan, E., Luz, B. (2007) Diffusivity fractionations of $H_2^{16}O/H_2^{17}O$ and $H_2^{16}O/H_2^{18}O$ in air and their implications for isotope hydrology. *Rapid Communications in Mass Spectrometry* 21, 2999–3005. https://doi.org/10.1002/rcm.3180

Berman, E.S.F., Levin, N.E., Landais, A., Li, S., Owano, T. (2013) Measurement of $\delta^{18}O$, $\delta^{17}O$, and ^{17}O-excess in Water by Off-Axis Integrated Cavity Output Spectroscopy and Isotope Ratio Mass Spectrometry. *Analytical Chemistry* 85, 10392–10398. https://doi.org/10.1021/ac402366t

Bright, J. (2009) Isotope and major-ion chemistry of groundwater in Bear Lake Valley, Utah and Idaho, with emphasis on the Bear River Range. In: Rosenbaum, J.G., Kaufman, D.S. (Eds.) *Paleoenvironments of Bear Lake, Utah and Idaho, and its catchment*. Geological Society of America, Boulder, Special Paper 450, 105–132. https://doi.org/10.1130/2009.2450(04)

Craig, H., Gordon, L.I. (1965) Deuterium and oxygen 18 variations in the ocean and marine atmosphere. In: Tongiorgi, E. (Ed.) *Stable Isotopes in Oceanographic Studies and Paleotemperatures*. Spoleto, Italy, 9–130.

Criss, R.E. (1999) *Principles of Stable Isotope Distribution*. Oxford University Press, New York. https://doi.org/10.1093/oso/9780195117752.001.0001

Custado, M.J., Gagnon, C.A., Belanger, B., Sekhon, N., Bernstein-Schalet, J., Kinsley, C.W., Sharp, W.D., Oster, J.L., Ibarra, D.E. (2025) Constraining the Modern Hydrological Balance of Bear Lake, Utah-Idaho: Insights From Stable Isotopes ($\delta^{18}O$ and $\delta^{2}H$). *Water Resources Research* 61, e2024WR038264. https://doi.org/10.1029/2024WR038264

Dean, W.E. (2009) Endogenic carbonate sedimentation in Bear Lake, Utah and Idaho, over the last two glacial-interglacial cycles. In: Rosenbaum, J.G., Kaufman, D.S. (Eds.) *Paleoenvironments of Bear Lake, Utah and Idaho, and its catchment*. Geological Society of America, Boulder, Special Paper 450, 169–196. https://doi.org/10.1130/2009.2450(07)

Gat, J.R. (1995) Stable Isotopes of Fresh and Saline Lakes. In: Lerman, A., Imboden, D.M., Gat, J.R. (Eds.) *Physics and Chemistry of Lakes*. Second Edition, Springer, Berlin, Heidelberg, 139–165. https://doi.org/10.1007/978-3-642-85132-2_5

Gázquez, F., Morellón, M., Bauska, T., Herwartz, D., Surma, J., *et al.* (2018) Triple oxygen and hydrogen isotopes of gypsum hydration water for quantitative paleo-humidity reconstruction. *Earth and Planetary Science Letters* 481, 177–188. https://doi.org/10.1016/j.epsl.2017.10.020

Gázquez-Sánchez, F., Jiménez-Espejo, F., Rodríquez-Rodríquez, M., Martegani, L., Voigt, C., *et al.* (2023) Roman water management impacted the hydrological functioning of wetlands during drought periods. *Scientific Reports* 13, 18815. https://doi.org/10.1038/s41598-023-46010-5

Gibson, J.J., Birks, S.J., Yi, Y. (2016) Stable isotope mass balance of lakes: a contemporary perspective. *Quaternary Science Reviews* 131, 316–328. https://doi.org/10.1016/j.quascirev.2015.04.013

Gonfiantini, R. (1986) Environmental Isotopes in Lake Studies. In: Fritz, P., Fontes, J.Ch. (Eds.) *Handbook of Environmental Isotope Geochemistry: Volume 2, The Terrestrial Environment, B*. Elsevier, Amsterdam, 113–168. https://doi.org/10.1016/B978-0-444-42225-5.50008-5

Gröning, M. (2011) Improved water $\delta^{2}H$ and $\delta^{18}O$ calibration and calculation of measurement uncertainty using a simple software tool. *Rapid Communications in Mass Spectrometry* 25, 2711–2720. https://doi.org/10.1002/rcm.5074

Hutchings, J.A., Konecky, B.L. (2023) Optimization of a Picarro L2140-i cavity ring-down spectrometer for routine measurement of triple oxygen isotope ratios in meteoric waters. *Atmospheric Measurement Techniques* 16, 1663–1682. https://doi.org/10.5194/amt-16-1663-2023

Ibarra, D.E., Kukla, T., Methner, K.A., Mulch, A., Chamberlain, C.P. (2021) Reconstructing Past Elevations From Triple Oxygen Isotopes of Lacustrine Chert: Application to the Eocene Nevadaplano, Elko Basin, Nevada, United States. *Frontiers in Earth Science* 9, 628868. https://doi.org/10.3389/feart.2021.628868

Katz, S.A., Levin, N.E., Rodbell, D.T., Gillikin, D.P., Aron, P.G., Passey, B.H., Tapia, P.M., Serrepe, A.R., Abbott, M.B. (2023) Detecting hydrologic distinctions among Andean lakes using clumped and triple oxygen isotopes. *Earth and Planetary Science Letters* 602, 117927. https://doi.org/10.1016/j.epsl.2022.117927

Kaufman, D.S., Bright, J., Dean, W.E., Rosenbaum, J.G., Moser, K., *et al.* (2009) A quarter-million years of paleoenvironmental change at Bear Lake, Utah and Idaho. In: Rosenbaum, J.G., Kaufman, D.S. (Eds.) *Paleoenvironments of Bear Lake, Utah and Idaho, and its catchment.* Geological Society of America, Boulder, Special Paper 450, 311–351. https://doi.org/10.1130/2009.2450(14)

Luz, B., Barkan, E. (2010) Variations of $^{17}O/^{16}O$ and $^{18}O/^{16}O$ in meteoric waters. *Geochimica et Cosmochimica Acta* 74, 6276–6286. https://doi.org/10.1016/j.gca.2010.08.016

Miller, M.F. (2002) Isotopic fractionation and the quantification of ^{17}O anomalies in the oxygen three-isotope system: an appraisal and geochemical significance. *Geochimica et Cosmochimica Acta* 66, 1881–1889. https://doi.org/10.1016/S0016-7037(02)00832-3

Passey, B.H., Ji, H. (2019) Triple oxygen isotope signatures of evaporation in lake waters and carbonates: A case study from the western United States. *Earth and Planetary Science Letters* 518, 1–12. https://doi.org/10.1016/j.epsl.2019.04.026

Passey, B.H., Levin, N.E. (2021) Triple Oxygen Isotopes in Meteoric Waters, Carbonates, and Biological Apatites: Implications for Continental Paleoclimate Reconstruction. *Reviews in Mineralogy and Geochemistry* 86, 429–462. https://doi.org/10.2138/rmg.2021.86.13

Pierchala, A., Rozanski, K., Dulinski, M., Gorczyca, Z. (2022) Quantification the diffusion-induced fractionation of $^{1}H_2{}^{17}O$ isotopologue in air accompanying the process of water evaporation. *Geochimica et Cosmochimica Acta* 322, 244–259. https://doi.org/10.1016/j.gca.2022.01.020

Steig, E.J., Jones, T.R., Schauer, A.J., Kahle, E.C., Morris, V.A., Vaughn, B.H., Davidge, L., White, J.W.C. (2021) Continuous-Flow Analysis of $\delta^{17}O$, $\delta^{18}O$, and δD of H_2O on an Ice Core from the South Pole. *Frontiers in Earth Science* 9, 640292. https://doi.org/10.3389/feart.2021.640292

Surma, J., Assonov, S., Bolourchi, M.J., Staubwasser, M. (2015) Triple oxygen isotope signatures in evaporated water bodies from the Sistan Oasis, Iran. *Geophysical Research Letters* 42, 8456–8462. https://doi.org/10.1002/2015GL066475

Surma, J., Assonov, S., Herwartz, D., Voigt, C., Staubwasser, M. (2018) The evolution of ^{17}O-excess in surface water of the arid environment during recharge and evaporation. *Scientific Reports* 8, 4972. https://doi.org/10.1038/s41598-018-23151-6

Terzer-Wassmuth, S., Wassenaar, L.I., Araguás-Araguás, L.J., Stumpp, C. (2023) Balancing precision and throughput of $\delta^{17}O$ and $\Delta'^{17}O$ analysis of natural waters by Cavity Ringdown Spectroscopy. *MethodsX* 10, 102150. https://doi.org/10.1016/j.mex.2023.102150

Uemura, R., Barkan, E., Abe, O., Luz, B. (2010) Triple isotope composition of oxygen in atmospheric water vapor. *Geophysical Research Letters* 37, L04402. https://doi.org/10.1029/2009GL041960

Voigt, C., Herwartz, D., Dorador, C., Staubwasser, M. (2021) Triple oxygen isotope systematics of evaporation and mixing processes in a dynamic desert lake system. *Hydrology and Earth System Sciences* 25, 1211–1228. https://doi.org/10.5194/hess-25-1211-2021

Voigt, C., Gázquez, F., Martegani, L., Sánchez Villanueva, A.I., Medina, A., Jiménez-Espinosa, R., Jiménez-Millán, J., Rodríguez-Rodríguez, M. (2025) How seasonal hydroclimate variability drives the triple oxygen and hydrogen isotope composition of small lake systems in semiarid environments. *Hydrology and Earth System Sciences* 29, 1783–1806. https://doi.org/10.5194/hess-29-1783-2025

Contrasting controls on $\delta^{18}O$-$\delta^{2}H$ and $\delta^{18}O$-$\delta^{17}O$ isotope systematics in a balance-filled lake

M.J. Custado, A.R. Waldeck, B. Belanger, X.-K. Wang, J.C.K. Rugenstein, K.M. Cobb, J.L. Oster, D.E. Ibarra

Supplementary Information

The Supplementary Information includes:

- Datasets and Code
- Physical and Hydroclimatic Setting of Bear Lake
- Isotope Notations
- Analytical and Data Reduction Methods
- Monte Carlo Implementation of the Lake Isotopic Mass Balance Equation
- Reconstruction of the $\delta^{18}O$ Composition of Unevaporated Catchment Precipitation ($\delta^{18}O_{rucp}$)
- Tables S-1 to S-6
- Figures S-1 to S-4
- Supplementary Information References

Datasets and Code

The isotopic dataset and Python scripts used for analysis and visualization can be found through the following link: https://doi.org/10.5281/zenodo.20819990. The master list spreadsheet file contains all data and geographic coordinates. The Python script used to reduce the Picarro L2140-i data output can be accessed through: https://doi.org/10.5281/zenodo.18356153.

Physical and Hydroclimatic Setting of Bear Lake

Situated within the northeastern Great Basin on the Utah-Idaho border, Bear Lake has been a critical water resource used for irrigation, flood management, and hydropower. Prior to around 1912, the lake was hydrologically disconnected from the Bear River, until an inlet canal was built to divert water to the lake which has since altered the lake's hydrology (Kaliser, 1972; Dean *et al.*, 2009). The lake is 32 km long with a maximum width of 12 km near the center. The lake's surface area is 282 km^2 at full capacity, with a maximum depth of 63 m and mean depth of 28 m (Birdsey, 1989; Dean

et al., 2009). The lake deepens from west to east, primarily due to the N-S trending fault on the eastern side of the lake (Dean *et al.*, 2009).

Chemical and hydrological changes in the lake since this diversion is detailed in Dean *et al.* (2007, 2009). Currently, Bear Lake is primarily an alkaline lake, with Ca^{2+}, Mg^{2+}, and HCO_3^- dominating the dissolved chemistry derived from the weathering of carbonate lithology in the Bear River Range (Fig. 1; Dean *et al.,* 2009). This region experiences hot, dry summer seasons and cold, wet winters, with evaporation still exceeding precipitation at annual basis, keeping the lake saturated with respect to carbonate minerals. Consequently, much of the water that enters the lake is in the form of snowmelt. This pronounced seasonality produces a distinct thermal and chemical stratification. During the late summer, specific conductance (25 °C) in the upper layers of the lake is approximately 685 µS cm^{-1}, increasing to approximately 700 µS cm^{-1} in the hypolimnion. The mean total dissolved solids (TDS) ranges from approximately 533 to 582 mg/L across the water column and similarly increase with depth (Dean *et al.*, 2007, 2009).

Isotope Notation

Raw isotope values (R) are the ratio of the rare isotope with the abundant isotope in the sample, normalized to the isotopic ratio of an internationally accepted standard. It is commonly reported using the delta (δ) notation and in per mil units (parts per thousand, ‰). The following equation is used to convert isotope ratios to δ values:

$$\delta = \left(\frac{R_{sample}}{R_{standard}} - 1\right) 1000 \qquad \text{Eq. S-1}$$

Analytical and Data Reduction Methods

The collected water samples were analysed for stable isotopes through cavity ring-down spectroscopy using a Picarro L2140-i unit. Three replicates of each sample were prepared in separate vials and were ran in different sequences. Following the protocols for memory and drift corrections from Hutchings and Konecky (2023), only the last three injections out of the six injections made for each vial were used in the data analysis. Additionally, we applied memory correction factors that were derived for the instrument from a separate analysis of internal standards. A linear regression of multiple replicates of an internal standard ("*Drift*") placed throughout the run sequence was used to correct for instrument drift. Internally calibrated ultrapure water was used as the drift correction standard.

Data were subsequently normalized using isotopically heavy and light internal standards (*"Heavy"* and *"Light,"* respectively) that bracket the isotopic range of the samples. These internal standards were calibrated against VSMOW2 and USGS reference materials (Table S-5). USGS46 standards were also analysed during each sequence to evaluate analytical accuracy (Table S-7).

The average of the last three injections per vial were taken as the $\delta^{17}O$, $\delta^{18}O$, and $\delta^{2}H$ data, while $\Delta'^{17}O$ was calculated for each injection using Eq. 4 before averaging. The final reported isotope values represent error-weighted averages of three measurement replicates (Eq. S-8).

Sample uncertainty calculations

Uncertainties for the $\delta^{17}O$, $\delta^{18}O$, and $\delta^{2}H$ data for each sample replicate were derived from the combined uncertainties of the calibrated internal standards and the standard deviations of the last three injections for each internal standard and sample following equation from Gröning (2011):

Eq. S-2

$$u(\delta_{sample}) = \left[\left(\frac{\partial f}{\partial \delta_{LS}}\right)^2 \cdot u(\delta_{LS})^2 + \left(\frac{\partial f}{\partial \delta_{HS}}\right)^2 \cdot u(\delta_{HS})^2 + \left(\frac{\partial f}{\partial \delta_{w\,LS}}\right)^2 \cdot u(\delta_{w\,LS})^2 + \left(\frac{\partial f}{\partial \delta_{w\,HS}}\right)^2 \cdot u(\delta_{w\,HS})^2 + \left(\frac{\partial f}{\partial \delta_{sample}}\right)^2 \cdot u(\delta_{sample})^2 \right]^{1/2}$$

where u is the reported (in the case for the internal standards) and measured uncertainties and δ is the reported or measured isotopic value. The subscripts correspond to either the sample, the calibrated value of the internal standards (*LS* for the light standard, and *HS* for the heavy standard). Terms with '*w*' as subscripts refer to the measured value of either HS or LS. The partial derivative terms are the variances of the different measurements and are calculated as:

$$\frac{\partial f}{\partial \delta_{LS}} = 1 - \frac{\delta_{sample} - \delta_{w\,LS}}{\delta_{w\,HS} - \delta_{w\,LS}} \quad \text{Eq. S-3}$$

$$\frac{\partial f}{\partial \delta_{HS}} = \frac{\delta_{sample} - \delta_{w\,LS}}{\delta_{w\,HS} - \delta_{w\,LS}} \quad \text{Eq. S-4}$$

$$\frac{\partial f}{\partial \delta_{w\,LS}} = \delta_{HS} - \delta_{LS} \cdot \frac{\delta_{sample} - \delta_{w\,LS}}{(\delta_{W\,HS} - \delta_{w\,LS})^2} - \frac{\delta_{HS} - \delta_{LS}}{\delta_{w\,HS} - \delta_{w\,LS}} \quad \text{Eq. S-5}$$

$$\frac{\partial f}{\partial \delta_{w\,LS}} = -(\delta_{HS} - \delta_{LS}) \cdot \frac{\delta_{sample} - \delta_{w\,LS}}{(\delta_{W\,HS} - \delta_{w\,LS})^2} \quad \text{Eq. S-6}$$

$$\frac{\partial f}{\partial \delta_{w\,sample}} = (\delta_{HS} - \delta_{LS}) \cdot \frac{\delta_{HS} - \delta_{LS}}{\delta_{w\,HS} - \delta_{w\,LS}} \quad \text{Eq. S-7}$$

The uncertainty for the $\Delta'^{17}O$ measurement of each sample replicate was determined by taking the standard error of the mean (SEM) from the last three injections. After calculating the uncertainties for each parameter, the error-weighted mean of each replicate measurement (x) was derived, along with their combined uncertainty (u). The following were the equations used:

$$x_{weighted\ average} = \frac{\sum w_i x_i}{\sum w_i} \quad \text{Eq. S-8}$$

$$u_{weighted\ average} = \frac{1}{\sqrt{\sum w_i}} \quad \text{Eq. S-9}$$

where the subscript *'i'* represent the replicates, and *w* as the weight of each replicate, calculated using:

$$w_i = \frac{1}{{u_i}^2} \quad \text{Eq. S-10}$$

The final reported uncertainty for $\Delta'^{17}O$ also accounts for the number of successful injections ($6 \leq n \leq 9$) to adjust for small-sample uncertainty. This was accomplished by multiplying the derived standard error of the mean by the appropriate Student's t-factor at 1σ for the corresponding degrees of freedom (BIPM *et al.*, 2008; Pierchala *et al.*, 2021).

Monte Carlo Implementation of the Lake Isotopic Mass Balance Equation

1. Parametrization

This section details how parameters and input distributions for the Monte Carlo calculations were set up to estimate the output values for humidity and X_e and their associated uncertainties.

1.1. Equilibrium and kinetic fractionation factors

The equilibrium fractionation factors (α_{eq}) for $\delta^{18}O$ and $\delta^{2}H$ are determined through empirical equations as functions of temperature (T), in Kelvin. In this work, we adopt the equations derived by Horita and Wesolowski (1994) using the convention where $\alpha_{eq} > 1$, representing the isotopic ratio in the liquid over the vapor:

$$10^3 ln\ \alpha_{eq}\ (^{18}O) = -7.685 + 6.7123\left(\frac{10^3}{T}\right) - 1.6664\left(\frac{10^6}{T^2}\right) + 0.35041\left(\frac{10^9}{T^3}\right) \quad \text{Eq. S-11}$$

$$10^3 ln\ \alpha_{eq}\ (^{2}H) = 1158.8\left(\frac{T^3}{10^9}\right) - 1620.1\left(\frac{T^2}{10^6}\right) + 794.84\left(\frac{T}{10^3}\right) - 161.04 + 2.9992\left(\frac{10^9}{T^3}\right) \quad \text{Eq. S-12}$$

We derive the equilibrium fractionation factor for $\delta^{17}O$ through its relationship with $\delta^{18}O$, using a θ value of 0.529 applied for equilibrium fractionation (Barkan and Luz, 2007):

$$^{17}\alpha_{eq} = \left(^{18}\alpha_{eq}\right)^{\theta} \quad \text{Eq. S-13}$$

Additionally, we adopt the following kinetic fractionation factors representing pure molecular diffusion (α_{diff}) of $\delta^{18}O$ and $\delta^{2}H$ experimentally derived by Merlivat (1978), and of $\delta^{17}O$ as calculated by Barkan and Luz (2007): α_{diff} ($\delta^{18}O$) = 1.0285, α_{diff} ($\delta^{2}H$) = 1.0251, and α_{diff} ($\delta^{17}O$) = 1.0146. Notably, α_{diff} ($\delta^{17}O$) can also be calculated theoretically from α_{diff} ($\delta^{18}O$) using Eq. S-13 and by applying a θ of 0.5185 (Barkan and Luz, 2007), yielding 1.0147, which closely resembles the experimentally derived value.

To account for turbulence in natural settings, an exponent of n = 0.5 is applied to the α_{diff} values (Horita, *et al.*, 2008), which accounts for the magnitude of kinetic fractionation occurring above open water bodies consistent with most lake studies (Gonfiantini, 1986; Gibson *et al.*, 2016a). The following are the values used as inputs to the calculations: α_{diff} ($\delta^{18}O$) = 1.0141, α_{diff} ($\delta^{2}H$) = 1.0125, and α_{diff} ($\delta^{17}O$) = 1.0073. Fig. S-3 shows the response of the modelled lake isotopic composition to varying *n* values.

1.2. Isotopic composition of atmospheric moisture (δ_A)

The isotopic composition of the atmospheric moisture is estimated by assuming an equilibrium isotopic exchange between precipitation and atmospheric moisture, as described by the following equation (Gibson *et al.*, 2016a):

$$\delta_A = \frac{\left(\delta_p - k\varepsilon^+\right)}{\left(1 + 10^{-3} \cdot k\varepsilon^+\right)} \quad \text{Eq. S-14}$$

where δ_P is the evaporation-flux weighted annual mean isotopic composition of precipitation, k is the seasonality factor, and ε^+ is equilibrium enrichment factor, defined as $1000(\alpha_{eq} - 1)$. The δ_P used in this study was derived from precipitation samples collected from Utah State University (USU) and Utah Valley University (UVU) campuses, with evaporation rate data extracted from the North American Regional Reanalysis (NARR, Mesinger *et al.*, 2006) dataset. Because monthly evaporation rates were explicitly accounted for, the influence of seasonality is inherently incorporated; hence we set the seasonality factor k to 1. Typical k values for temperate climates are ~0.75 to correct for seasonality when mean annual precipitation isotopic composition is used (Gibson *et al.*, 2016a, 2016b). Custado *et al.* (2025) quantified a 76% separation between δ_A derived from the mean annual δ_P, which estimates equilibrium enrichment (ε^+) and δ_A derived from the δ_P that accounts for evaporation rates, which is the effective equilibrium enrichment ($\varepsilon_{effective}$; Gibson *et al.*, 2016a).

1.3. Probability distributions of input parameters

Inflow (δ_I) and lake (δ_S) isotopic composition

We adopt a pure Monte Carlo method for generating input distributions for the inflow and lake isotopic composition to capture the spread within the measured samples for each input parameter (Davis *et al.*, 2015). Specifically for this work, we constructed our input distributions based on Gaussian mixture modelling (GMM) concepts (Terejanu *et al.*, 2008; McLachlan *et al.*, 2019), transforming each data point into normal distributions centred on the observed value with its variance defined by their corresponding analytical uncertainty. The final input distributions are effectively empirical Gaussian mixtures, as they are generated by equally sampling from the measurement-based normal distributions through Monte Carlo methods. This method explicitly propagates analytical uncertainty and limits assumptions on the underlying distribution for each isotopic parameter, considering the temporal and sample size limitations of our dataset. This is particularly important for $\Delta'^{17}O$ whose reported analytical uncertainties can reach up to 15 to 20 per meg.

The input distribution for the inflow isotopic composition is generated by constructing separate distributions for each inflow component: inlet (n = 1), creeks (n = 18), groundwater (n = 6), and precipitation (n = 19). The components are then averaged by using the volumetric contribution of each component to the lake as the weighing factor. For the lake isotopic composition, input distribution is generated from data from 7 measured samples.

Evaporation flux-weighted isotopic composition of precipitation (δ_P)

Input distributions for evaporation flux-weighted precipitation were constructed to explicitly preserve covariance of $\delta^{18}O$ to $\delta^{17}O$ and $\delta^{2}H$ following the Global Meteoric Water Line (GMWL). This reflects the assumption that precipitation is largely influenced by mass-dependent equilibrium fractionation processes during condensation and Rayleigh distillation, which strongly influence individual isotopes but limits variability in the slope, particularly relative to the deviation observed in surface waters (Dansgaard, 1964; Luz and Barkan, 2010; Aron *et al.*, 2021).

First, normal distributions of $\Delta'^{17}O$ and d-excess were generated from the mean and combined uncertainties of the measured precipitation samples. These distributions were then used to generate $\delta^{17}O$ and $\delta^{2}H$ values from $\delta^{18}O$ values via Equations 4 and 5 in the main text, explicitly preserving the GMWL relationship (Eqs. 4 and 5 in the main text). Additional noise from the spread of the measured $\delta^{17}O$ and $\delta^{2}H$ values and their corresponding analytical uncertainties were incorporated into the distributions.

Probability distribution for evaporation flux-weighted temperature

A normal distribution for temperature centred on the evaporation flux-weighted temperature was generated whose spread is based on the weighted variance of the monthly temperature data extracted from the NARR dataset. We chose normal distributions for most of the parameters as a reasonable first-order approximation of the variability in the available datasets.

2. Model implementation

For each isotopic system, relative humidity and X_e are calculated simultaneously by applying the mass balance equation (Eq. 1 in the main text) to each isotope, forming a system of two nonlinear equations for both $\delta^{18}O$-$\delta^{2}H$ (one equation each for $\delta^{18}O$ and $\delta^{2}H$) and triple oxygen (one equation each for $\delta^{17}O$ and $\delta^{18}O$). The constructed systems of equations are then solved using the Python scientific computing library (SciPy; Virtanen *et al.*, 2020). Specifically, the calculations were implemented using the *fsolve* function within SciPy's *optimize* package, which employs a modified Powell's hybrid method. This optimization algorithm iteratively solves systems of nonlinear equations by combining Gauss-Newton methods with gradient descent, allowing for rapid convergence and numerical stability (Powell, 1970).

Monte Carlo simulations are implemented by generating distributions of the input parameters with 100, 000 realizations. The lake mass balance calculations are performed for each realization to estimate relative humidity and X_e values and their associated uncertainties. All calculations are executed using Python scripts available through the link provided in the *Datasets and code* section.

3. Sensitivity analysis

The sensitivities of lake isotopic composition, relative humidity, and X_e to variations in isotopic and environmental (temperature and relative humidity) parameters were evaluated using the same Monte Carlo implementation of the lake mass balance calculations. Normal distributions (n = 100,000) of the input parameters were generated based on the median values and interquartile ranges (IQR) calculated from the initial Monte Carlo simulations. Similar to the treatment of evaporation flux-weighted precipitation, the covariance between among the isotopes was preserved assuming that large-scale atmospheric variability is governed primarily by mass-dependent equilibrium fractionation and mixing, following the GMWL. To systematically limit extreme outputs while keeping the inputs within plausible values, the generated normal distributions were truncated within one standard deviation, retaining realizations that are within the 15.9th and 84.1st percentiles.

The sensitivity of the lake isotopic composition was evaluated at three X_e values (0, 0.3, and 1) with humidity, temperature, and the isotopic compositions of inflow and atmospheric moisture serving as inputs. Meanwhile, the sensitivity of relative humidity and X_e parameters was evaluated with respect to variations in temperature and the isotopic compositions of inflow, lake, and atmospheric moisture.

Reconstruction of the $\delta^{18}O$ Composition of Unevaporated Catchment Precipitation ($\delta^{18}O_{rucp}$)

The equations for the reconstruction of the isotopic composition of the source are adopted from the work of Passey and Ji (2019) and Katz *et al.* (2023):

$$\lambda_{lake} = A \times \left(\Delta'^{17}O_{lake}\right)^3 + B \times \left(\Delta'^{17}O_{lake}\right)^2 + C \times \Delta'^{17}O_{lake} + D \quad \text{Eq. S-15}$$

$$\delta'^{18}O_{rucp} = \frac{\Delta'^{17}O_{MWL} - \delta'^{17}O_{lake} + (\lambda_{lake} - \lambda_{ref})\delta'^{18}O_{lake}}{\lambda_{lake} - \lambda_{ref}} \quad \text{Eq. S-16}$$

where λ_{lake} represents the slope in $\delta'^{17}O$-$\delta'^{18}O$ space between the source and lake waters. The subscripts lake, MWL (Meteoric Water Line), and rucp (reconstructed unevaporated catchment precipitation) denote the water whose isotopic composition is used in the calculation. We assume that the MWL has a slope of $\lambda_{ref} = 0.528$ and an intercept of $\Delta'^{17}O$ = 32 per meg (Passey and Ji, 2019).

Eq. S-15 is the general form of the polynomial that fit the data from modelled $\Delta'^{17}O$ and λ_{lake} values based on isotopic data from the western United States (Passey and Ji, 2019) and later expanded with other lake datasets (Katz *et al.*, 2023). Table S-5 summarizes the coefficients (A, B, C, D) derived from these modelling exercises.

Supplementary Tables

Table S-1 Volumetric discharge value of each inflow component used in the calculations.

Parameter	Value	Uncertainty*	Calculation	Data source*
Upstream (through inlet canal) (f_U, m^3/yr)	3.18 x 10^8	3 to 6%	Mean	USGS
Creeks (f_C, m^3/yr)	1.45 x 10^8	3 to 6%	Mean	USGS and Utah DEQ
Precipitation (f_P, m^3/yr)	1.08 x 10^8	-	Mean	NARR
Groundwater (f_g, m^3/yr)	7.62 x 10^4	1.6 to 2.3%	-	Custado *et al.* (2025)

**Estimated uncertainty values for United States Geological Survey (USGS) discharge measurements from Sauer and Meyer (1992); estimated groundwater flux uncertainty from Custado et al. (2025).*
*** USGS and Utah Department of Environment Quality (Utah DEQ) retrieved from the National Water Interface System (NWIS) database (USGS, 2024); North American Regional Reanalysis (NARR; Mesinger et al., 2006)*

Table S-2 Distributions of input parameters used for the Monte Carlo calculations.

Parameter	Isotope	Input distribution (Fig. S-1)	Mean	Standard deviation	Median	IQR*		Reference data
Temperature (°C)	-	Normal	11.119	8.147	11.124	5.640 – 16.624		Evaporation flux weighted; NWS** data
α_{eq}	$\delta^{18}O$	Normal	1.011	0.001	1.011	1.010 – 1.011		Calculated from temperature (Eq. S-11)
	$\delta^{17}O$	Normal	1.006	0.0004	1.006	1.005 – 1.006		Calculated from α_{eq} ($\delta^{18}O$) (θ = 0.529, Eq. S-13)
	$\delta^{2}H$	Normal	1.096	0.011	1.095	1.088 – 1.103		Calculated from temperature (Eq. S-12)
α_{diff}	$\delta^{18}O$	n.a.	1.014	n.a.	n.a.	n.a.		Kinetic fractionation at zero humidity; 1.0285^{n}, where n = 0.5 (Merlivat, 1978; Voigt *et al.*, 2021)
	$\delta^{17}O$	n.a.	1.007	n.a.	n.a.	n.a.		Kinetic fractionation at zero humidity; 1.0146^{n}, where n = 0.5 (Merlivat, 1978; Voigt *et al.*, 2021)
	$\delta^{2}H$	n.a.	1.012	n.a.	n.a.	n.a.		Kinetic fractionation at zero humidity; 1.0251^{n}, where n = 0.5 (Merlivat, 1978; Voigt *et al.*, 2021)
Total inflow	$\delta^{18}O$ (‰)	Non-normal	-15.479	0.848	-15.603	-16.167 – -14.927		Measured inlet, creeks, amount-weighed precipitation, groundwater, and spring samples
	$\Delta'^{17}O$ (per meg)	Normal (slightly skewed)	19.636	7.630	19.250	14.302 – 24.719		
	$\delta^{2}H$ (‰)	Non-normal	-116.471	6.445	-117.481	-121.496 – -112.074		

**Interquartile Range, range between the 25th and 75th percentile in the distribution*
***National Weather Station (https://www.ncdc.noaa.gov/cdo-web/), Lifton pump station in Idaho (42.123, -111.3133)*

Table S-2 continued.

Parameter	Isotope	Input distribution (Fig. S-1)	Mean	Standard deviation	Median	IQR*		Reference data
Precipitation	$\delta^{18}O$ (‰)	Normal	-11.122	3.340	-11.120	-13.371 – -8.860		Evaporation flux-weighted; Measured precipitation samples
	$\Delta'^{17}O$ (per meg)	Normal	35.064	22.017	35.058	20.142 – 49.914		
	$\delta^{2}H$ (‰)	Normal	-82.808	36.846	-82.743	-107.686 – -57.910		
Atmospheric moisture	$\delta^{18}O$ (‰)	Normal	-21.548	3.382	-21.546	-23.849 – -19.259		Calculated from evaporation flux-weighted precipitation (Eq. S-14)
	$\Delta'^{17}O$ (per meg)	Normal	35.064	22.017	35.058	9.556 – 39.314		
	$\delta^{2}H$ (‰)	Normal	-163.209	10.910	-162.977	-186.545 – -139.720		
Lake	$\delta^{18}O$ (‰)	Non-normal	-9.098	0.101	-9.095	-9.189 – -8.999		Measured lake samples
	$\Delta'^{17}O$ (per meg)	Normal	-2.892	9.878	-2.525	-8.732 – 3.582		
	$\delta^{2}H$ (‰)	Near normal	-84.789	0.492	-84.768	-85.185 – -84.403		

**Interquartile Range, range between the 25th and 75th percentile in the distribution*
***National Weather Station (https://www.ncdc.noaa.gov/cdo-web/), Lifton pump station in Idaho (42.123, -111.3133)*

Table S-3 Summary statistics of output distributions

Parameter	Isotope system	Output distribution (Fig. S-2)	Mean	Standard deviation	Median	IQR*
Relative humidity	Triple oxygen	Non-normal	0.561	0.251	0.590	0.375 – 0.774
	$\delta^{18}O$-$\delta^{2}H$	Non-normal	0.607	0.235	0.639	0.455 – 0.788
Evaporation/ Inflow (X_e)	Triple oxygen	Skewed normal	0.292	0.114	0.267	0.231 – 0.308
	$\delta^{18}O$-$\delta^{2}H$	Skewed normal	0.294	0.112	0.281	0.240 – 0.321

**Interquartile Range, range between the 25th and 75th percentile in the distribution*

Table S-4 Monthly climatological means of climate data used.

Month	Relative humidity, %	Evaporation, kg/m^2	Precipitation rate, kg/m^2/s	Temperature, °F
Jan	-	0.050	1.12E-05	18.4
Feb	-	0.069	1.30E-05	19.4
Mar	-	0.118	1.09E-05	28.6
Apr	63.91	0.204	1.44E-05	39.1
May	64.18	0.340	1.64E-05	49.3
Jun	62.39	0.455	1.20E-05	59.3
Jul	53.70	0.409	8.31E-06	68
Aug	59.00	0.274	8.77E-06	65
Sep	56.48	0.155	1.26E-05	55.8
Oct	61.99	0.084	1.35E-05	43.7
Nov	72.48	0.068	1.27E-05	31.2
Dec	-	0.049	1.23E-05	21

**Relative humidity data were extracted from USGS Station 415941111175401 (41.99471667, −111.2984667) and span May 2022 to November 2024; no data were reported for January, February, March, and December. The evaporation flux-weighted relative humidity cited in the main text was calculated assuming that months without data were fully saturated (h = 1), representing an upper-bound limit for these months. Evaporation and precipitation rates were obtained from the North American Regional Reanalysis (NARR) dataset; temperature data were obtained from the Lifton Pumping Station, ID (https://www.ncdc.noaa.gov/cdo-web/; 42.123, −111.315), covering the period 2000–2024. Lake stations marked as stars in Fig. 1b.*

Table S-5 $\delta^{18}O_{rucp}$ reconstructions using different coefficients (A, B, C, D) derived by Katz *et al.* (2023) and Passey and Ji (2019). These coefficients are applied to Eq. S-15.

λ_{lake}*	$\delta^{18}O_{rucp}$ (‰)*	A	B	C	D	Humidity range	Equation used
0.5228	-15.670 (IQR: -16.155 – -15.241)	9.8941	1.2759	0.0580	0.5229	Full (0.3 to 0.9)	Katz *et al.* (2023)
0.5235	-16.842 (IQR: -17.539 – -16.243)	1.9600	0.5340	0.0599	0.5237	Low (0.3 to 0.7)	Katz *et al.* (2023)
0.5213	-14.265 (IQR: -14.629 – -13.942)	40.9869	1.9363	0.0701	0.5215	High (0.7 to 0.9)	Katz *et al.* (2023)
0.5234	-16.672 (IQR: -17.340 – -16.095)	1.9856	0.5730	0.0601	0.5236	Western US (0.3 to 0.7)	Passey and Ji (2019)
0.5246	-18.066 (IQR: -21.261 – -15.851)	-	-	-	-	-	Inflow and lake data

**Median and IQR values are from 100,000 Monte Carlo simulations. The IQRs for the calculated λ_{lake} values are 0.0026 (Inflow and lake data) and 0.0007 (Passey and Ji, 2019, Katz et al., 2023).*

Table S-6 External standards used for the calibration of internal reference standards (VSMOW2, USGS53, USGS47) and data quality check (USGS46).

Standard	$\delta^{17}O$ (‰)	$\delta^{17}O$ uncertainty	$\delta^{18}O$ (‰)	$\delta^{18}O$ uncertainty	$\delta^{2}H$ (‰)	$\delta^{2}H$ uncertainty	Reference
VSMOW2	0	0.03	0	0.02	0	0.4	IAEA, 2017
USGS53	2.85	0.01	5.47	0.03	40.2	0.4	USGS, 2018; Berman *et al.*, 2013
USGS46	-15.85	0.02	-29.8	0.03	-235.9	0.7	USGS, 2019a, Berman *et al.*, 2013
USGS47	-10.47	0.02	-19.8	0.02	-150.2	0.5	USGS, 2019b; Hutchings and Konecky, 2023

Table S-7 Internal standards used for data normalization and drift correction. The $\Delta'^{17}O$ of each replicate was calculated from the $\Delta'^{17}O$ value of each of the last three injections.

Standard	Date	$\delta^{17}O$ (‰)	$\delta^{17}O$ (1σ, ‰,)	$\delta^{18}O$ (‰)	$\delta^{18}O$ (1σ, ‰,)	$\delta^{2}H$ (‰)	$\delta^{2}H$ (1σ, ‰,)	$\Delta'^{17}O$ (per meg)	$\Delta'^{17}O$ (SEM, per meg)	*n* replicates
Heavy	6/7/2024	2.640	0.028	5.039	0.024	2.967	0.193	-19.351	10.858	2
Light	6/7/2024	-8.711	0.027	-16.395	0.022	-97.684	0.327	-26.343	11.397	2
Drift	6/7/2024	-2.000	0.015	-3.794	0.015	-16.451	0.133	-16.811	3.355	6
USGS46	6/7/2024	-15.689	0.056	-29.491	0.048	-228.800	0.813	-5.984	20.100	2
Heavy	6/9/2024	2.625	0.031	5.016	0.023	2.967	0.185	-22.855	10.099	2
Light	6/9/2024	-8.706	0.033	-16.392	0.020	-97.679	0.313	5.416	9.869	2
Drift	6/9/2024	-2.014	0.015	-3.786	0.013	-16.516	0.111	-4.066	7.602	6
USGS46	6/9/2024	-15.578	0.046	-29.315	0.031	-227.517	0.785	4.888	15.677	2
Heavy	6/11/2024	2.622	0.036	5.020	0.046	2.929	0.220	-32.852	7.553	2
Light	6/11/2024	-8.727	0.046	-16.417	0.052	-97.673	0.379	-27.389	10.186	2
Drift	6/11/2024	-1.984	0.016	-3.791	0.021	-16.634	0.129	-3.500	2.174	6
USGS46	6/11/2024	-15.776	0.060	-29.576	0.073	-228.458	0.859	-39.039	5.770	2
Heavy	6/14/2024	2.621	0.018	5.000	0.016	2.953	0.176	-40.110	18.083	2
Light	6/14/2024	-8.700	0.025	-16.350	0.031	-97.518	0.320	-38.770	4.999	2
Drift	6/14/2024	-2.022	0.020	-3.809	0.015	-16.218	0.155	-6.708	6.802	6
USGS46	6/14/2024	-15.683	0.039	-29.512	0.057	-228.298	0.803	47.843	25.414	2
Heavy	6/17/2024	2.626	0.036	5.020	0.029	2.963	0.289	-22.050	16.298	2
Light	6/17/2024	-8.748	0.018	-16.417	0.016	-97.800	0.328	3.567	15.616	2
Drift	6/17/2024	-1.992	0.019	-3.803	0.014	-16.658	0.161	6.526	5.402	6
USGS46	6/17/2024	-15.590	0.034	-29.352	0.033	-226.589	0.760	14.081	8.120	2
Heavy	6/20/2024	2.631	0.058	5.071	0.085	3.036	0.399	-21.232	15.567	2
Light	6/20/2024	-8.716	0.034	-16.395	0.019	-97.680	0.339	-24.346	14.607	2
Drift	6/20/2024	-1.970	0.022	-3.728	0.026	-16.224	0.190	18.910	8.695	6
USGS46	6/20/2024	-15.702	0.043	-29.564	0.042	-229.235	0.716	17.417	5.846	2

Supplementary Figures

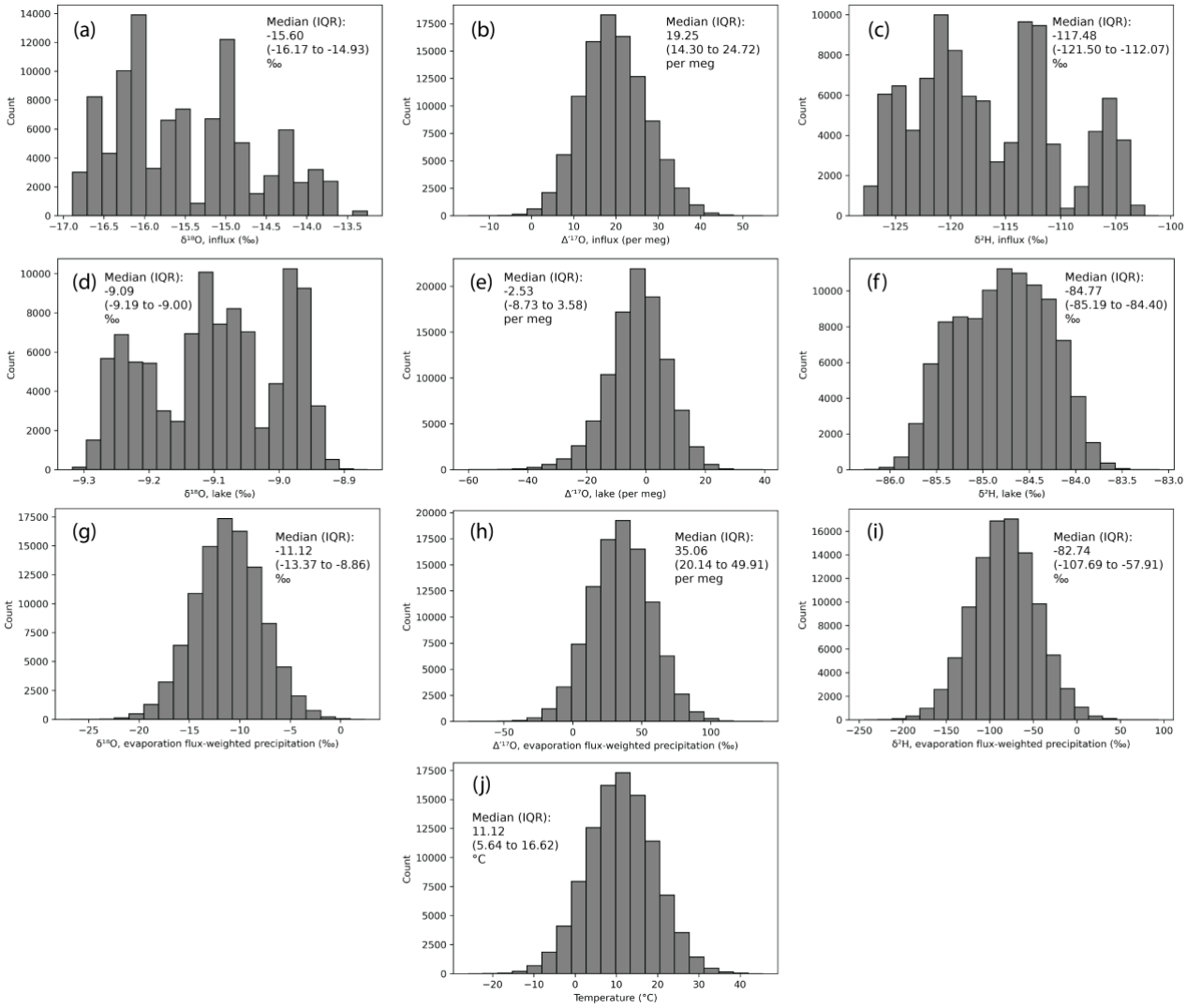

Figure S-1 Histograms of the generated input distributions as described in the Parametrization section (n = 100,000). From top left, proceeding horizontally: **(a)** $\delta^{18}O$ of influx, **(b)** $\Delta'^{17}O$ of influx, **(c)** $\delta^{2}H$ of influx, **(d)** $\delta^{18}O$ of lake, **(e)** $\Delta'^{17}O$ of lake, **(f)** $\delta^{2}H$ of lake, **(g)** $\delta^{18}O$ of evaporation flux-weighted precipitation, **(h)** $\Delta'^{17}O$ of evaporation flux-weighted precipitation, **(i)** $\delta^{2}H$ of evaporation flux-weighted precipitation, and **(j)** temperature.

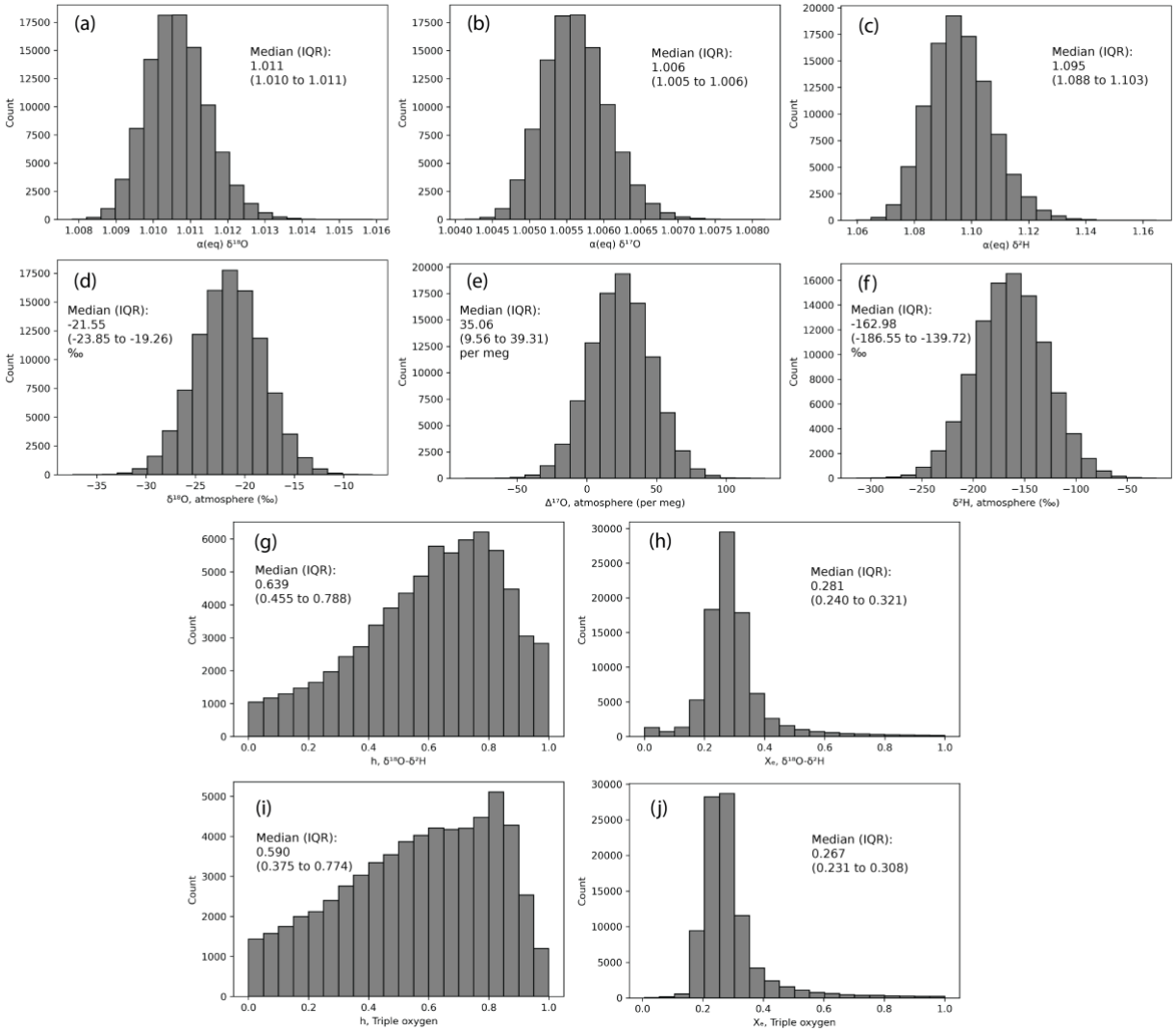

Figure S-2 Histograms of the calculated output distributions from Monte Carlo simulations of the isotopic lake mass balance (n = 100,000). From top left, proceeding horizontally: Equilibrium fractionation factors (α_{eq}) calculated from the range of input temperatures for **(a)** $\delta^{18}O$, **(b)** $\delta^{17}O$, and **(c)** $\delta^{2}H$; **(d)** atmospheric moisture isotopic compositions for **(d)** $\delta^{18}O$, **(e)** $\Delta'^{17}O$, and **(f)** $\delta^{2}H$; calculated **(g)** humidity and **(h)** X_e in the $\delta^{18}O$- $\delta^{2}H$ space; calculated **(i)** humidity and **(j)** X_e in the triple oxygen space.

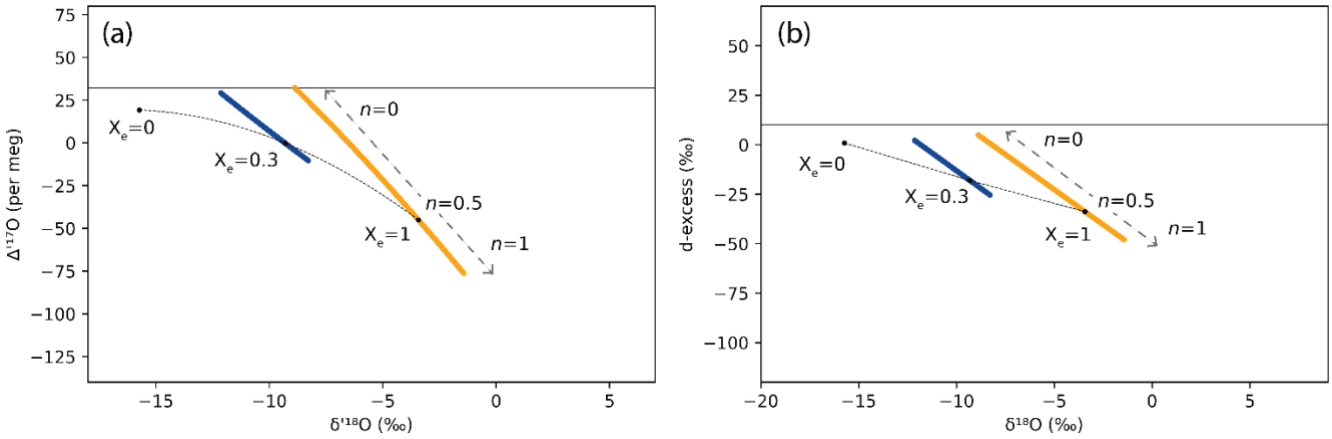

Figure S-3 Sensitivity plots of the lake isotopic composition to the turbulence parameter (n) in the **(a)** triple oxygen ($\delta'^{18}O$ vs. $\Delta'^{17}O$) and **(b)** $\delta^{18}O$-$\delta^{2}H$ ($\delta^{18}O$ vs. d-excess) spaces at increasing X_e. The value of n was varied from 0 (turbulent diffusion endmember; $\alpha_{diff} = 1$) to 1 (molecular diffusion endmember; $\alpha_{diff} = 1.0285$ for $\delta^{18}O$, 1.0251 for $\delta^{2}H$, and 1.0146 for $\delta^{17}O$; Merlivat, 1978; Barkan and Luz, 2007). Gray dashed lines indicate the direction of change in lake isotopic composition. Because direct constraints on n were not available for Bear Lake, we adopted the commonly used value of n = 0.5 and focused the Monte Carlo analysis of the isotopic parameters. As n approaches 1, corresponding to increasingly molecular diffusion-dominated transport, lake waters become isotopically heavier in $\delta^{18}O$ and lighter in $\Delta'^{17}O$ and d-excess, reflecting enhanced kinetic fractionation. Conversely, as n approaches 0, the term $\alpha_{eq}\alpha_{diff}$ in Eq. 1 approaches α_{eq}, indicating the breakdown of the laminar boundary layer described in the Craig–Gordon model and the increasing dominance of turbulent transport.

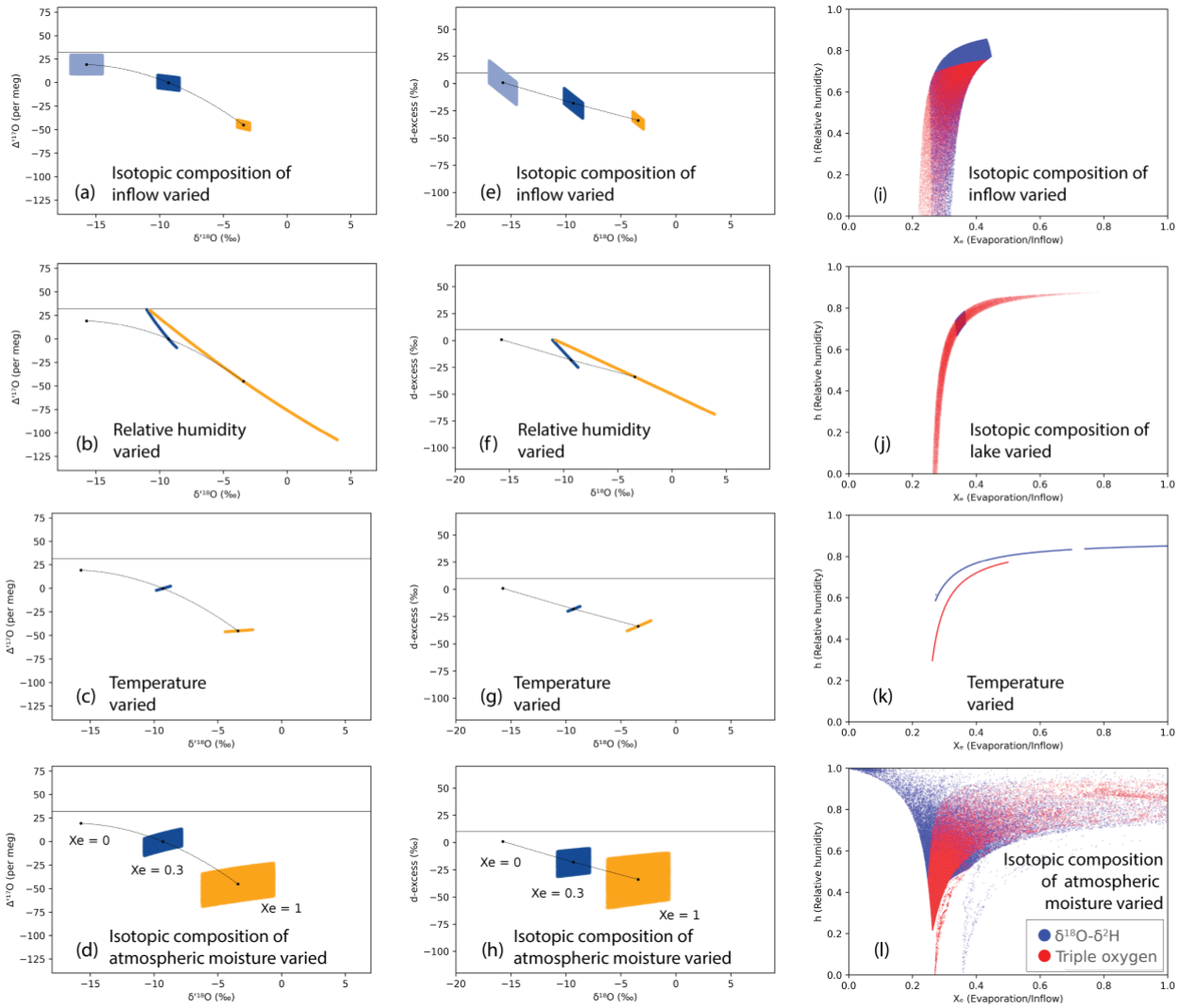

Figure S-4 Sensitivity plots of the lake isotopic composition in the triple oxygen ($\delta'^{18}O$ vs. $\Delta'^{17}O$, left column) and $\delta^{18}O$-$\delta^{2}H$ ($\delta^{18}O$ vs. d-excess, middle column) spaces, and sensitivity of relative humidity and X_e in both isotopic systems (X_e vs. h, right column). The lake isotopic composition is simulated for X_e values of 0, 0.3, and 1; lines represent evaporation trajectory based on the available isotopic data. The left and middle columns illustrate changes in lake isotopic composition as individual input parameters are varied (with all others held constant): **(a, e)** inflow isotopic composition, **(b, f)** relative humidity, **(c, g)** temperature, and **(d, h)** atmospheric moisture isotopic composition. Right column shows changes in relative humidity and X_e with the following parameters held constant: **(i)** inflow isotopic composition, **(j)** lake isotopic composition, **(k)** temperature, and **(l)** atmospheric moisture isotopic composition. All plots are derived from Monte Carlo mass balance simulations (n = 100,000) using normally distributed input parameters.

Supplementary Information References

Aron, P.G., Levin, N.E., Beverly, E.J., Huth, T.E., Passey, B.H., Pelletier, E.M., Poulsen, C.J., Winkelstern, I.Z., Yarian, D.A. (2021) Triple oxygen isotopes in the water cycle. *Chemical Geology* 565, 120026. https://doi.org/10.1016/j.chemgeo.2020.120026

Barkan, E., Luz, B. (2007) Diffusivity fractionations of $H_2{}^{16}O/H_2{}^{17}O$ and $H_2{}^{16}O/H_2{}^{18}O$ in air and their implications for isotope hydrology. *Rapid Communications in Mass Spectrometry* 21, 2999–3005. https://doi.org/10.1002/rcm.3180

Berman, E.S.F., Levin, N.E., Landais, A., Li, S., Owano, T. (2013) Measurement of $\delta^{18}O$, $\delta^{17}O$, and ^{17}O-excess in Water by Off-Axis Integrated Cavity Output Spectroscopy and Isotope Ratio Mass Spectrometry. *Analytical Chemistry* 85, 10392–10398. https://doi.org/10.1021/ac402366t

BIPM, IEC, IFCC, ILAC, ISO, IUPAC, IUPAP, OIML (2008) *Evaluation of measurement data — Guide to the expression of uncertainty in measurement*. First Edition, Joint Committee for Guides in Metrology.

Birdsey, P. (1989) *The Limnology of Bear Lake, Utah-Idaho, 1912-1988: A Literature Review*. Utah Department of Natural Resources, Publication 89-5, Salt Lake City.

Custado, M.J., Gagnon, C.A., Belanger, B., Sekhon, N., Bernstein-Schalet, J., Kinsley, C.W., Sharp, W.D., Oster, J.L., Ibarra, D.E. (2025) Constraining the Modern Hydrological Balance of Bear Lake, Utah-Idaho: Insights From Stable Isotopes ($\delta^{18}O$ and $\delta^{2}H$). *Water Resources Research* 61, e2024WR038264. https://doi.org/10.1029/2024WR038264

Dansgaard, W. (1964) Stable isotopes in precipitation. *Tellus* 16, 436–468. https://doi.org/10.1111/j.2153-3490.1964.tb00181.x

Davis, P., Syme, J., Heikoop, J., Fessenden-Rahn, J., Perkins, G., Newman, B., Chrystal, A.E., Hagerty, S.B. (2015) Quantifying uncertainty in stable isotope mixing models. *Journal of Geophysical Research: Biogeosciences* 120, 903–923. https://doi.org/10.1002/2014JG002839

Dean, W.E., Forester, R.M., Bright, J., Anderson, R.Y. (2007) Influence of the diversion of Bear River into Bear Lake (Utah and Idaho) on the environment of deposition of carbonate minerals. *Limnology and Oceanography* 52, 1094–1111. https://doi.org/10.4319/lo.2007.52.3.1094

Dean, W.E., Wurtsbaugh, W.A., Lamarra, V.A. (2009) Climatic and limnologic setting of Bear Lake, Utah and Idaho. In: Rosenbaum, J.G., Kaufman, D.S. (Eds.) *Paleoenvironments of Bear Lake, Utah and Idaho, and its catchment*. Geological Society of America, Boulder, Special Paper 450, 1–14. https://doi.org/10.1130/2009.2450(01)

Gibson, J.J., Birks, S.J., Yi, Y. (2016a) Stable isotope mass balance of lakes: a contemporary perspective. *Quaternary Science Reviews* 131, 316–328. https://doi.org/10.1016/j.quascirev.2015.04.013

Gibson, J.J., Birks, S.J., Yi, Y., Moncur, M.C., McEachern, P.M. (2016b) Stable isotope mass balance of fifty lakes in central Alberta: Assessing the role of water balance parameters in determining trophic status and lake level. *Journal of Hydrology: Regional Studies* 6, 13–25. https://doi.org/10.1016/j.ejrh.2016.01.034

Gonfiantini, R. (1986) Environmental Isotopes in Lake Studies. In: Fritz, P., Fontes, J.Ch. (Eds.) *Handbook of Environmental Isotope Geochemistry: Volume 2, The Terrestrial Environment, B*. Elsevier, Amsterdam, 113–168. https://doi.org/10.1016/B978-0-444-42225-5.50008-5

Gröning, M. (2011) Improved water $\delta^{2}H$ and $\delta^{18}O$ calibration and calculation of measurement uncertainty using a simple software tool. *Rapid Communications in Mass Spectrometry* 25, 2711–2720. https://doi.org/10.1002/rcm.5074

Horita, J., Wesolowski, D.J. (1994) Liquid-vapor fractionation of oxygen and hydrogen isotopes of water from the freezing to the critical temperature. *Geochimica et Cosmochimica Acta* 58, 3425–3437. https://doi.org/10.1016/0016-7037(94)90096-5

Horita, J., Rozanski, K., Cohen, S. (2008) Isotope effects in the evaporation of water: a status report of the Craig–Gordon model. *Isotopes in Environmental and Health Studies* 44, 23–49. https://doi.org/10.1080/10256010801887174

Hutchings, J.A., Konecky, B.L. (2023) Optimization of a Picarro L2140-i cavity ring-down spectrometer for routine measurement of triple oxygen isotope ratios in meteoric waters. *Atmospheric Measurement Techniques* 16, 1663–1682. https://doi.org/10.5194/amt-16-1663-2023

IAEA (2017) *Reference Sheet for International Meaurement Standards*. International Atomic Energy Agency, Vienna.

Kaliser, B.N. (1972) *Environmental Geology of Bear Lake Area, Rich County, Utah*. Utah Geological and Mineralogical Survey, Bulletin 096, Salt Lake City.

Katz, S.A., Levin, N.E., Rodbell, D.T., Gillikin, D.P., Aron, P.G., Passey, B.H., Tapia, P.M., Serrepe, A.R., Abbott, M.B. (2023) Detecting hydrologic distinctions among Andean lakes using clumped and triple oxygen isotopes. *Earth and Planetary Science Letters* 602, 117927. https://doi.org/10.1016/j.epsl.2022.117927

Luz, B., Barkan, E. (2010) Variations of $^{17}O/^{16}O$ and $^{18}O/^{16}O$ in meteoric waters. *Geochimica et Cosmochimica Acta* 74, 6276–6286. https://doi.org/10.1016/j.gca.2010.08.016

McLachlan, G.J., Lee, S.X., Rathnayake, S.I. (2019) Finite Mixture Models. *Annual Review of Statistics and Its Application* 6, 355–378. https://doi.org/10.1146/annurev-statistics-031017-100325

Merlivat, L. (1978) Molecular diffusivities of $H_2{}^{16}O$, $HD^{16}O$, and $H_2{}^{18}O$ in gases. *The Journal of Chemical Physics* 69, 2864–2871. https://doi.org/10.1063/1.436884

Mesinger, F., DiMego, G., Kalnay, E., Mitchell, K., Shafran, P.C., *et al.* (2006) North American Regional Reanalysis. *Bulletin of the American Meteorological Society* 87, 343–360. https://doi.org/10.1175/BAMS-87-3-343

Passey, B.H., Ji, H. (2019) Triple oxygen isotope signatures of evaporation in lake waters and carbonates: A case study from the western United States. *Earth and Planetary Science Letters* 518, 1–12. https://doi.org/10.1016/j.epsl.2019.04.026

Pierchala, A., Rozanski, K., Dulinski, M., Gorczyca, Z., Czub, R. (2021) Triple-isotope calibration of in-house water standards supplemented by determination of ^{17}O content of USGS49-50 reference materials using cavity ring-down laser spectrometry. *Isotopes in Environmental and Health Studies* 57, 254–261. https://doi.org/10.1080/10256016.2021.1875222

Powell, M.J.D. (1970) A Hybrid Method for Nonlinear Equations. In: Rabinowitz, P. (Ed.) *Numerical Methods for Nonlinear Algebraic Equations*. Gordon and Breach Science, London, 87–144.

Sauer, V.B., Meyer, R.W. (1992) *Determination of error in individual discharge measurements*. U.S. Geological Survey, Norcross, GA, Open-File Report 92-144. https://doi.org/10.3133/ofr92144

Terejanu, G., Singla, P., Singh, T., Scott, P.D. (2008) Uncertainty Propagation for Nonlinear Dynamic Systems Using Gaussian Mixture Models. *Journal of Guidance, Control, and Dynamics* 31, 1623–1633. https://doi.org/10.2514/1.36247

USGS (2018) *Report of Stable Isotopic Composition: Reference Material USGS53*. U.S. Geological Survey, Reston.

USGS (2019a) *Report of Stable Isotopic Composition - Reference Material USGS46*. U.S. Geological Survey, Reston.

USGS (2019b) *Report of Stable Isotopic Composition - Reference Material USGS47*. U.S. Geological Survey, Reston.

USGS (2024) USGS Current Water Data for the Nation. Accessed 10 April 2024. https://waterdata.usgs.gov/

Virtanen, P., Gommers, R., Oliphant, T.E., Haberland, M., Reddy, T., *et al.* (2020) SciPy 1.0: fundamental algorithms for scientific computing in Python. *Nature Methods* 17, 261–272. https://doi.org/10.1038/s41592-019-0686-2

Voigt, C., Herwartz, D., Dorador, C., Staubwasser, M. (2021) Triple oxygen isotope systematics of evaporation and mixing processes in a dynamic desert lake system. *Hydrology and Earth System Sciences* 25, 1211–1228. https://doi.org/10.5194/hess-25-1211-2021